

1 **Reply to reviewers**

2 **Referee 1**

3 On my comment on the assumption of phase states used in thermodynamic model calculations, I suggest 1> the  
4 authors to add Figure R1 in the authors' responses to the supplement; and, 2> make clear which phase state is  
5 assumed in the calculations.

6  
7 **Re: Good suggestion. We have added the Figure R1 in the supplement. And we stated that in this study,**  
8 **the phase state was assumed to be stable in the model calculation in line 190-191.**

9  
10  
11 **Referee 2**

12 Regarding my last comment, "Line 320 (and 370), I am not sure whether using PNSD is proper here. The ALWC  
13 depends on the amount of hygroscopic materials, no matter which sizes they are present." I think that the authors  
14 did not address explicitly. Maybe my comment is not fully clear.  
15 My point is that the ALWC mainly depends on the amount (mass) of hygroscopic materials, no matter which  
16 sizes these materials are present, either in Aiken mode or in accumulation mode. The Kelvin effect has only  
17 minimal influence on ALWC for particles in the Aiken mode and accumulation mode range. Therefore, the  
18 PNSD does not influence ALWC directly.

19  
20 **Re: Thanks for the reviewer's comment. As you stated, we also found the influence of Kelvin effect to**  
21 **ALWC is small. However, the PNSD is still important to ALWC. This is because the particles in**  
22 **different sizes have different hygroscopicity. We found most hygroscopic materials were distributed in**  
23 **accumulation mode. In this paper, three factors (PNSD, ambient RH, aerosol chemical composition)**  
24 **to ALWC were discussed. It's obvious that PNSD and aerosol chemical composition determine the**  
25 **distribution and mass concentration of hygroscopic materials. So PNSD is an important factor for**  
26 **ALWC although it does not influence ALWC directly. Therefore, the effect of PNSD on ALWC was**  
27 **discussed here, as followed by the method in Bian et al. (2014) and Tan et al. (2017).**

28 **For avoiding confusion, we added: "PNSD does not influence ALWC directly, but it's an important**  
29 **factor to determine the mass concentration and distribution of hygroscopic materials." in Line339-340.**

30  
31  
32  
33  
34 **Reference:**

35 Bian, Y. X., Zhao, C.S., Ma, N., Chen, J., Xu, W.Y.: A study of aerosol liquid water content based on hygroscopicity  
36 measurements at high relative humidity in the North China Plain, Atmos. Chem. Phys., 14 (12), 6417–6426,  
37 <https://doi.org/10.5194/acp-14-6417-2014>, 2014.

38 Tan, H., Cai, M., Fan, Q., Liu, L., Li, F., & Chan, P. W., et al.: An analysis of aerosol liquid water content and related  
39 impact factors in pearl river delta, Science of The Total Environment, 579, 1822-1830,  
40 <https://doi.org/10.1016/j.scitotenv.2016.11.167>, 2017.

41  
42  
43  
44  
45  
46  
47  
48  
49

50  
51  
52  
53

54 **Significant contribution of organics to aerosol liquid water content in**  
55 **winter in Beijing, China**

56  
57

58 **Xiaoai Jin<sup>1</sup>, Yuying Wang<sup>1,2</sup>, Zhanqing Li<sup>3</sup>, Fang Zhang<sup>1</sup>, Weiqi Xu<sup>4,5</sup>, Yele Sun<sup>4,5</sup>, Xinxin Fan<sup>1</sup>,**  
59 **Guangyu Chen<sup>6</sup>, Hao Wu<sup>1</sup>, Jingye Ren<sup>1</sup>, Qiuyan Wang<sup>2</sup>, and Maureen Cribb<sup>3</sup>**

60  
61

62 <sup>1</sup>State Key Laboratory of Remote Sensing Science, College of Global Change and Earth System Science, Beijing Normal University,  
63 Beijing 100875, China

64 <sup>2</sup>Key Laboratory for Aerosol-Cloud-Precipitation of China Meteorological Administration, School of Atmospheric Physics, Nanjing  
65 University of Information Science and Technology, Nanjing 210044, China

66 <sup>3</sup>Department of Atmospheric and Oceanic Science, and Earth System Science Interdisciplinary Center, University of Maryland, College  
67 Park, MD, USA

68 <sup>4</sup>State Key Laboratory of Atmospheric Boundary Layer Physics and Atmospheric Chemistry, Institute of Atmospheric  
69 Physics, Chinese Academy of Sciences, Beijing 100029, China

70 <sup>5</sup>College of Earth Sciences, University of Chinese Academy of Sciences, Beijing 100049, China

71 <sup>6</sup>Zhejiang Windey Co., Ltd., Hangzhou 310012, China

72

73 Correspondence to: Zhanqing Li ([zli@atmos.umd.edu](mailto:zli@atmos.umd.edu)), Yuying Wang ([wyy\\_bnu@126.com](mailto:wyy_bnu@126.com))

74

75

76

77

78 **Abstract**

79

80 The aerosol liquid water content (ALWC), an important component of atmospheric particles, has a  
81 significant effect on atmospheric optical properties, visibility and multiphase chemical reactions. In  
82 this study, ALWC is determined from aerosol hygroscopic growth factor and particle number size  
83 distribution (PNSD) measurements and also simulated by the ISORROPIA II thermodynamic model  
84 with measured aerosol chemical composition data at an urban site in Beijing from 8 November to 15  
85 December 2017. Rich measurements made during the experiment concerning virtually all aerosol  
86 properties allow us not only to derive the ALWC but also to study the contributions by various species  
87 for which little has been done in this region. The simulated ALWC including the contribution of  
88 organics and the calculated ALWC are highly correlated (coefficient of determination  $R^2 = 0.92$ ). The  
89 ALWC contributed by organics ( $ALWC_{Org}$ ) accounts for  $30 \% \pm 22 \%$  of the total ALWC during the  
90 sampling period. These results suggest a significant contribution of organics to ALWC, which is rather  
91 different from previous studies that showed negligible contributions by organics. Our results also show  
92 that ALWC correlates well with the mass concentrations of sulfate, nitrate, and secondary organic  
93 aerosols (SOA) ( $R^2 = 0.66, 0.56, \text{ and } 0.60$ , respectively). We further noted that accumulation mode  
94 particles play a key role in determining ALWC, dominating among all the aerosol modes. ALWC is an  
95 exponential function of ambient relative humidity (RH) whose strong diurnal variation influence the  
96 diurnal variation of ALWC. However, there is a three-hour lag between the extremes of ALWC and  
97 RH values, due to the diurnal variations in PNSD and aerosol chemical composition. Finally, a case  
98 study reveals that  $ALWC_{Org}$  plays an important role in the formation of secondary aerosols through  
99 multiphase reactions at the initial stage of a heavy haze episode.

100

101

102

## 103 1. Introduction

104 China has experienced rapid economic developments during the past few decades, resulting in  
105 frequent heavy haze events. Severe air pollution may harm human health and affect the regional  
106 climate through aerosol direct and indirect radiation effects (Li et al., 2016; G. X. Wu et al., 2016; [Wei](#)  
107 [et al., 2019a](#); [Wei et al., 2019b](#)). However, air pollution formation mechanisms and aerosol climate  
108 effects remain highly uncertain due to the complex physical and chemical processes involved (Tao et  
109 al., 2012; Y. Wang et al., 2014).

110 Aerosol liquid water (ALW), a component of atmospheric particles in the atmosphere, exists  
111 universally and plays an important role in many atmospheric physical and chemical processes (Nguyen  
112 et al., 2016). For example, ALW can influence aerosol optical properties, resulting in increased  
113 extinction coefficients, lowered atmospheric visibilities, enhanced aerosol optical depths (AODs), and  
114 changes in the direct climatic effect of aerosols (Dougle et al., 1996; Adams et al., 2001; Liao et al.,  
115 2005; Seinfeld and Pandis, 2006). Secondary aerosols (SA) are considered to be the main source of  
116 particulate pollution during heavy haze events in China (Huang et al., 2014). Many studies now  
117 highlight the significance of aerosol liquid water content (ALWC) in the formation of SA through  
118 chemical reactions (e.g., Arellanes et al., 2006; G. Wang et al., 2016; Cheng et al., 2016). This is  
119 because ALW can dilute the absolute concentration of solutes, adjust aerosol acidity, and serve as a  
120 reactant, resulting in increases in trace gas (e.g.,  $\text{N}_2\text{O}_5$  and  $\text{HO}_2$ ) uptake coefficients (Wahner et al.,  
121 1998; Bertram et al., 2009; Abbatt et al., 2012). H. Wang et al. (2017) found that the uptake coefficient  
122 of  $\text{N}_2\text{O}_5$  can be high, which is related to high ALWC in Beijing, thereby increasing the formation of  
123 nitrates. ALW can also speed up the aqueous phase chemical reaction by serving as a reactor for the  
124 transformation of  $\text{SO}_2$  to sulfate (Zheng et al., 2015; G. Wang et al., 2016; Cheng et al., 2016). Some  
125 studies have found that ALWC can facilitate the formation of secondary organic aerosols (SOA)  
126 through aqueous-phase chemistry and photochemistry (Blando et al., 2001; Surratt et al., 2007;  
127 Hennigan et al., 2008; Song et al., 2019). Furthermore, observations in Beijing have shown that

128 aqueous-phase processes play a dominant role in the additional formation of oxidized SOA (Xu et al.,  
129 2017). Overall, investigating the formation of SA and haze in North China requires an examination of  
130 ALWC and its factors including aerosol particle number size distribution (PNSD), aerosol chemical  
131 composition and ambient related humidity (RH) in this region.

132 However, directly measuring real-time ALWC is not feasible yet because of technical limitations,  
133 (Kuang et al., 2018). Four indirect methods have been proposed to calculate real-time ALWC: (1) the  
134 aerosol PNSD under dry conditions and ambient RH conditions are first measured, then ALWC is  
135 calculated as the difference between dry and ambient aerosol volumes (Stanier et al., 2004); (2) the  
136 increased aerosol volume due to water uptake (i.e., ALWC) is calculated according to the measured  
137 dry PNSD, size-dependent aerosol hygroscopicity, and ambient RH (Kitamori et al., 2009; Bian et al.,  
138 2014; Tan et al., 2017); (3) the dry and ambient aerosol volumes are first estimated using the measured  
139 aerosol optical enhancement and Ångström exponent, then ALWC is calculated as the difference  
140 between dry and ambient aerosol volumes (Kuang et al., 2018); and (4) ALWC is simulated using  
141 thermal equilibrium models such as the ISORROPIA thermodynamic model (Nenes et al., 1998),  
142 Aerosol Inorganics Model models (Wexler and Clegg, 2002), the Simulating Composition of  
143 Atmospheric Particles in Equilibrium model (Kim et al., 1993), and the Gibb's Free Energy  
144 Minimization model (Ansari et al., 1999) with aerosol chemical composition information as input.

145 ALWC mostly depends on aerosol PNSD, chemical composition, and ambient RH. Hodas et al.  
146 (2014) reported that ALWC in the Po Valley in Italy was driven by locally formed anthropogenic  
147 nitrates. The implications for the lifetimes of water-soluble organic compounds and its potential  
148 influence on SOA formation were also discussed. Another study also revealed that ALWC in Beijing  
149 was driven by secondary inorganic aerosols (SIA; Z. Wu et al., 2018). Most previous studies have  
150 focused on the interaction between inorganic salts and ALWC, but the impact of organic species on  
151 ALWC been ignored to our knowledge (Blando et al., 2001; Surratt et al., 2007; Hennigan et al., 2008;  
152 Carlton et al., 2014). A thorough understanding of the association of ALWC with organic aerosols in

153 the atmosphere is lacking.

154 In this study, ALWC is calculated using the indirect method (2) and simulated using the  
155 ISORROPIA II model, i.e., indirect method (4), discussed previously. The effects of inorganic aerosols,  
156 organic aerosols, PNSD, and ambient RH on ALWC are then investigated separately. We demonstrate  
157 the significant contribution of organics to ALWC in Beijing and provide evidence that the ALW  
158 contributed by organics serves as a reactor for sulfate and SOA formation.

## 159 **2. Data and measurements**

### 160 **2.1. Sampling site**

161 The Air Pollution and Human Health (APHH) winter field campaign took place from 8 November  
162 to 15 December 2016 at the Chinese Academy of Sciences' Institute of Atmospheric Physics Tower  
163 Branch in Beijing. Beijing is located in the northwest part of the North China Plain, which has  
164 experienced rapid economic developments during the last few decades. A large amount of gaseous  
165 precursors and other air pollutants are emitted in this region every year, causing serious air pollution  
166 problems. The sampling site is located in the northwestern urban area of Beijing (39.97°N, 116.37°E),  
167 between the north third and fourth ring roads and surrounded by restaurants. Traffic and cooking  
168 emissions are thus the main pollutants at the site. Aerosols at this site can, therefore, well represent  
169 anthropogenic aerosols in highly polluted areas. Sun et al. (2013) and Y. Wang et al. (2017) provide  
170 more detailed descriptions of the sampling site.

### 171 **2.2. Instrumentation**

172 Sampling instruments used during the field campaign included a scanning mobility particle sizer  
173 (SMPS) equipped with a long differential mobility analyzer (DMA; model 3081A, TSI) and a  
174 condensation particle counter (CPC; model 3772, TSI). A custom-built hygroscopicity tandem  
175 differential mobility analyzer (H-TDMA) was installed in an air-conditioned mobile container at

176 ground level. The temperature inside the container was maintained at 20–25°C. A high-resolution  
177 aerosol mass spectrometer (HR-AMS) was set up in a sampling room located on a two-story roof,  
178 about 25 m north from the container. Sampled air went through a PM<sub>2.5</sub> cyclone inlet fixed on the top  
179 of the container before entering the instruments. The RH of the sampled air was dried to below 20 %  
180 by a dryer system consisting of a tube filled with silica gel and a Nafion dryer (model PD-70T-24ss,  
181 Perma Pure Inc., USA). Various meteorological parameters, including wind speed (WS), wind  
182 direction (WD), temperature (*T*), and RH, were measured from a 325-m meteorological tower located  
183 ~20 m west of the container. In this study, all times are reported in Beijing local time (UTC+8 h).

184 PNSDs with electrical-mobility diameters ranging from 10 to 600 nm were measured by a  
185 scanning mobility particle sizer (SMPS) at a 5-min time resolution. PNSDs were extended to diameters  
186 ranging from 0.6 to 1 μm by fitting the measured PNSDs with functions consisting of three-mode log-  
187 normal distributions (Hussein et al., 2005). Thus generated are PNSDs with a diameter range of 10 nm  
188 to 1 μm.

189 The H-TDMA system developed by the Guangzhou Institute of Tropical and Marine Meteorology  
190 measured the size-dependent aerosol hygroscopic growth factor (GF). The H-TDMA system mainly  
191 consists of four parts. The first part is a Nafion dryer to keep the RH of sampled air below 20 % and a  
192 bipolar neutralizer (soft X-ray, model 3088, TSI Inc.) to equilibrate the particle charge (Wiedensohler  
193 et al., 1988). Next, the sampled air passes through the first differential mobility analyzer (DMA1;  
194 model 3081L, TSI Inc.) to produce mono-dispersed particles. In this study, the diameters were set to  
195 40, 80, 110, 150, and 200 nm. The sampled air then went through a Nafion humidifier (model PD-70T-  
196 24ss, Perma Pure Inc., USA) used to humidify the RH of sampled air to 90 %. The last part of the H-  
197 TDMA is the second DMA (same model as the DMA1) and a water-based condensation particle  
198 counter (model 3787, TSI Inc.), used to measure the number size distribution of humidified particles  
199 in the five selected diameters. Y. Wang et al. (2017) provide a detailed introduction to the H-TDMA  
200 system.

201 Size-resolved non-refractory sub-micron aerosol chemical species, including organics (Org),  
202 sulfate ( $\text{SO}_4^{2-}$ ), nitrate ( $\text{NO}_3^-$ ), ammonium ( $\text{NH}_4^+$ ), and chloride ( $\text{Cl}^-$ ), were measured by the HR-AMS.  
203 The sampled air dried by diffusion silica gel dryers was drawn into the HR-AMS through a  $\text{PM}_{2.5}$   
204 cyclone inlet to remove coarse particles larger than 2.5  $\mu\text{m}$ . The HR-AMS was calibrated with pure  
205 ammonium nitrate following the procedures detailed in Jimenez et al. (2003). Sun et al. (2016b)  
206 provide operational details about the HR-AMS.

### 207 3. Method

#### 208 3.1. ALWC calculation based on H-TDMA measurements

209 The ALWC is calculated based on measurements of the aerosol GF and particle number size  
210 distribution. Briefly, H-TDMA data are first used to derive the size-resolved particle GFs at various  
211 RHs. Then ALWC is calculated as the increased aerosol volume due to hygroscopic growth attributed  
212 to water uptake.

213 Chen et al. (2012) showed how to calculate size-resolved particle GFs at different RHs. First, a  
214 three-mode log-normal distribution is applied to fit the measured PNSD to produce fitting parameters  
215 for each mode. The hygroscopicity parameter ( $\kappa$ ) in any mode is assumed to be constant. The H-  
216 TDMA-derived size-dependent  $\kappa$  can then be used to deduce the corresponding  $\kappa$  for the nucleation  
217 mode, the Aitken mode, and the accumulation mode of PNSDs according to the following equation:

$$218 \quad \kappa(D_p) = \frac{\sum_{i=1}^3 \kappa_i N_i(D_p)}{\sum_{i=1}^3 N_i(D_p)}, \quad (1)$$

219 where  $\kappa_i$  refers to the  $\kappa$  of the  $i$ th mode, and  $N_i(D_p)$  refers to the number concentration of particles in  
220 the  $i$ th mode. According to  $\kappa$ -Köhler theory (Petters and Kreidenweis, 2007),  $\kappa$  at a certain diameter  
221 ( $D_d$ ) can be calculated as

$$222 \quad \kappa(D_d) = (\text{GF}^3 - 1) \cdot \left[ \frac{1}{\text{RH}} \exp\left(\frac{4\sigma_{s/a} M_w}{RT \rho_w D_d \text{GF}}\right) - 1 \right], \quad (2)$$

223 where RH is the control value by the humidifier in the H-TDMA system,  $T$  is the mean room



224 temperature of the container set to 293 K,  $\sigma_{s/a}$  is the surface tension of the solution/air interface assumed  
225 to be the same as the surface tension coefficient between water and air (about 0.0728 N m<sup>-1</sup> at 293 K),  
226  $M_w$  is the molecular weight of water,  $R$  is the universal gas constant,  $\rho_w$  is the density of water, and  $D_d$   
227 is the diameter of the dry particles. The GF at a given RH is defined as the ratio of the humidified  
228 diameter [ $D_p$ (RH)] to  $D_d$ :

$$229 \quad \text{GF} = D_p(\text{RH})/D_d . \quad (3)$$

230 The known  $\kappa$  of each mode derives the size-resolved  $\kappa$  at 90 % RH using Eq. (1). Substituting the size-  
231 resolved  $\kappa$  into Eq. (2) results in size-resolved GFs at various RHs. Finally, the volume of ALWC at  
232 ambient RH is equal to the increased aerosol volume due to water uptake, i.e., ALWC can be calculated  
233 as

$$234 \quad \text{ALWC}_{\text{HTDMA}} = \left[ \frac{1}{6} \sum_i n_i D_{p,i}^3 \left( \text{GF}(D_{p,i}, \text{RH})^3 - 1 \right) \right] \cdot \rho_w , \quad (4)$$

235 where  $n_i$  refers to the particle number concentration of dry particles for the corresponding particle size  
236 range in the  $i$ th mode, and  $D_{p,i}$  refers to the particle diameter for the corresponding particle size range.

### 237 3.2. ALWC simulations based on the ISORROPIA II model

238 The thermodynamic equilibrium model ISORROPIA II developed by Fountoukis and Nenes  
239 (2007) using aerosol chemical composition information from the HR-AMS can simulate ALWC  
240 (ALWC<sub>ISO</sub>). The bulk chemical composition was used in the model. However, the ISORROPIA II  
241 model only considers the contribution of inorganic species (Ca<sup>2+</sup>, K<sup>+</sup>, Mg<sup>2+</sup>, NH<sup>+</sup>, Na<sup>+</sup>, SO<sub>4</sub><sup>2-</sup>, NO<sub>3</sub><sup>-</sup>,  
242 Cl<sup>-</sup> and H<sub>2</sub>O) on ALWC and neglects the contribution of organics. In this study, the model was set up  
243 to reverse mode due to the lack of measurements of gaseous ammonia, and the phase state was assumed  
244 to be stable in the model calculation. [As shown in Figure S1, the simulated ALWC in stable mode is](#)  
245 [similar to that in metastable mode \( \$R^2 = 0.99\$ \).](#) ~~and~~

246 According to the model assumptions that the aerosol curvature effect in Köhler theory is ignored,  
247 and the aerosol water uptake has no effect on ambient vapor pressure, the water activity ( $a_w$ ) defined

248 as the effective mole fraction of water is equal to the ambient RH in this model (Seinfeld and Pandis,  
249 2006):

$$250 \quad a_w = RH \quad (5)$$

251 The ALWC can be calculated using the Zdanovskii–Stokes–Robinson (ZSR) mixing rule (Stokes and  
252 Robinson, 1966),

$$253 \quad ALWC_{ISO} = \sum_i \frac{M_i}{m_{0i}(a_w)}, \quad (6)$$

254 where  $M_i$  is the mole concentration of the  $i$ th species ( $\text{mol m}^{-3}$  in air), and  $m_{0i}(a_w)$  is the corresponding  
255 molality of the binary solution of the  $i$ th species under the same  $a_w$  with complex solution. Finally,  
256 with measured ambient RH and  $T$  values as input  $ALWC_{ISO}$  values under different RH and  $T$  conditions  
257 can be derived.

### 258 3.3. Inferring the contribution of organics to ALWC

259 According to the  $\kappa$ -Köhler theory and the ZSR mixing rule,  $\kappa$  can also be expressed as the sum of  
260 the contributions of each aerosol component:

$$261 \quad \kappa = \sum_i \varepsilon_i \kappa_i, \quad (7)$$

262 where  $\varepsilon_i$  and  $\kappa_i$  are the volume fraction and hygroscopicity of the  $i$ th species, respectively. Submicron  
263 aerosols mainly consist of organic and inorganic species (Carbone et al., 2013; Zieger et al., 2017). As  
264 mentioned in section 2.2, the HR-AMS measures the mass concentrations of organics and inorganics,  
265 including  $\text{SO}_4^{2-}$ ,  $\text{NO}_3^-$ ,  $\text{NH}_4^+$ , and Cl. The volume fraction of inorganic species can be calculated based  
266 on the ion-pairing scheme given by the following equations (Gysel et al., 2007):

$$267 \quad n_{\text{NH}_4\text{NO}_3} = n_{\text{NO}_3^-},$$

$$268 \quad n_{\text{NH}_4\text{HSO}_4} = \min(2n_{\text{SO}_4^{2-}} - n_{\text{NH}_4^+} + n_{\text{NO}_3^-}, n_{\text{NH}_4^+} - n_{\text{NO}_3^-}),$$

$$269 \quad n_{(\text{NH}_4)_2\text{SO}_4} = \max(n_{\text{NH}_4^+} - n_{\text{NO}_3^-} - n_{\text{SO}_4^{2-}}, 0),$$

$$\begin{aligned}
 n_{H_2SO_4} &= \max(0, n_{SO_4^{2-}} - n_{NH_4^+} + n_{NO_3^-}), \\
 n_{HNO_3} &= 0,
 \end{aligned}
 \tag{8}$$

270 where  $n$  represents the mole numbers, and “min” and “max” are minimum and maximum values,  
 271 respectively. The  $\kappa$  values of the inorganic species sulfuric acid, ammonium sulfate, ammonium  
 272 hydrogen sulfate, and ammonium nitrate are 1.19, 0.48, 0.56, and 0.58, respectively (Topping et al.,  
 273 2005; Petters and Kreidenweis, 2007). So the ZSR model can be used to estimate the contribution of  
 274 inorganic species to the  $\kappa$  value. In this paper, the chloride was not taken into account in ion-pairing  
 275 because its source is hard to determine. This may result in a minor uncertainty in  $\kappa$  calculation. The  
 276 hygroscopicity parameter of organics ( $\kappa_{Org}$ ) can be calculated using the volume fraction of organics  
 277 and the total  $\kappa$  value derived from the H-TDMA, according to Eq. (7). Finally, the ALWC contributed  
 278 by organic species ( $ALWC_{Org}$ ) can be calculated as (Petters and Kreidenweis, 2007)

$$ALWC_{Org} = \frac{m_{Org} \rho_w}{\rho_{Org}} \frac{\kappa_{Org}}{\left(\frac{1}{RH} - 1\right)},
 \tag{9}$$

281 where  $m_{Org}$  is the organic mass concentration from the AMS (Xu et al., 2015), and  $\rho_{Org}$  is the density  
 282 of organics, taken as  $1.4 \text{ g cm}^{-3}$  (Moore et al., 2011; Latham et al., 2013; Cerully et al., 2014).

## 284 4. Results and discussion

### 285 4.1. Comparison of calculated and simulated ALWC

286 The trends in ALWC calculated based on the hygroscopic growth factor and PNSD  
 287 ( $ALWC_{HTDMA}$ ) and simulated from ISOPPOPIA II model ( $ALWC_{ISO}$ ) are generally consistent. Figure  
 288 1a shows that  $ALWC_{HTDMA}$  and  $ALWC_{ISO}$  agree well and that their coefficient of determination ( $R^2$ )  
 289 is 0.89. The correlation is especially strong for RH over 90 %. However, for RH below 60 %,  $ALWC_{ISO}$   
 290 is less than  $ALWC_{HTDMA}$  and even close to 0 in some cases. Bian et al. (2014) and Tan et al. (2017)  
 291 observed a similar phenomenon in northern and southern China. There are three possible explanations  
 292 for these results. H-TDMA samples were humidified to 90 % RH during the field campaign, thereby  
 293 leading to the neglect of the deliquescence process in the  $ALWC_{HTDMA}$  calculation. This may lead to

294 overestimation of  $ALWC_{HTDMA}$  for RH below the deliquescence relative humidity (DRH). Second, the  
295 assumption of constant  $\kappa$  in each mode may lead to small uncertainty in size-resolved GFs at different  
296 RHs, resulting in small deviation in ALWC calculation. This may be another reason for the difference  
297 between  $ALWC_{HTDMA}$  and  $ALWC_{ISO}$ . In addition, the ISORROPIA II model ignores the effect of  
298 aerosol shape and complex organic species on the DRH. Previous studies have suggested that the  
299 particle spherical assumption and simplified aerosol chemical species in this model can overestimate  
300 the DRH (Seinfeld and Pandis, 2006; Sjogren et al., 2007). So for RH below the simulated DRH  
301 (~60 %), particles may still be dry in the ISORROPIA II model, but may have been hydrated in the  
302 real atmosphere. Therefore, this model underestimates ALWC. The ambient aerosol deliquescent  
303 phenomenon is rare in the North China Plain (Kuang et al., 2016). In addition, the ISORROPIA II  
304 model cannot simulate water uptake by organics, which can lead to some bias between simulated and  
305 calculated ALWCs. As described in section 3.3,  $ALWC_{Org}$  can be inferred and used to discuss  
306 differences between  $ALWC_{ISO}$  and  $ALWC_{HTDMA}$ . Figure 1b shows that adding  $ALWC_{Org}$  to  $ALWC_{ISO}$   
307 leads to a stronger correlation with  $ALWC_{HTDMA}$  ( $R^2 = 0.92$ ). The correlation improves significantly  
308 for RH below 60 %. This demonstrates that (1) organic species contribute significantly to ALWC, and  
309 (2) the underestimation of ALWC by the ISORROPIA II model is also related to the neglect of organic  
310 species in the model.

311

## 312 **4.2. Impact of different factors on ALWC**

### 313 **4.2.1. Impact of aerosol chemical species on ALWC**

314 Figure 2 shows the characteristics of seven heavy pollution events selected for examination.  
315 Figures 2a and 2c display the time series of WS, WD, and ambient RH. The prevailing wind during  
316 the haze episodes was a weak southerly wind that was favorable for bringing in pollutants from the  
317 highly populated and industrialized neighboring regions to the sampling site. This is beneficial to the

318 formation and accumulation of SA (T. Wang et al., 2010; Y. Wang et al., 2017). However, the prevailing  
319 winds during the clean events were strong northerly winds that always carried in a clean air mass,  
320 resulting in pollutants being quickly removed (Figure 2c). Note that the PM<sub>1</sub> mass concentration  
321 decreases somewhat in the evening during haze episodes, following the short-term change of WD from  
322 southerly to northerly. This is related to mountain-valley breezes in Beijing (Wehner et al., 2008; Gao  
323 et al., 2011; Y. Wang et al., 2017). These results demonstrate that heavy haze episodes have a strong  
324 correlation with local wind direction in Beijing.

325 Figures 2a and 2d show the time series of ambient RH and mass concentrations of aerosol chemical  
326 species in PM<sub>1</sub>. These figures suggest that the increase in inorganic and organic aerosols is  
327 synchronous with the increase in ambient RH during the heavy pollution periods (P1-P7). This is likely  
328 because of a positive feedback mechanism driven by Henry's law and thermodynamic equilibrium (Z.  
329 Wu et al., 2018). Figure 2b also shows that ALWC continuously increases during the pollution  
330 accumulation period. On average, ALWC increases from 8 to 89  $\mu\text{g m}^{-3}$  as ambient RH increases from  
331 15 to 80 %, and the inorganic and organic aerosol mass concentrations increase from 15 to 120  $\mu\text{g m}^{-3}$   
332 and from 12 to 78  $\mu\text{g m}^{-3}$ , respectively. These results imply that the increase in ambient RH and  
333 aerosol mass concentration are all important for the increase in ALWC.

334 Equation (4) also suggests that the absolute value of ALWC is dependent on the value of ambient  
335 RH and aerosol chemical composition (i.e., the GF value). To further investigate the impact of  
336 chemical composition on ALWC, the impact of RH on ALWC should be accounted for. Previous  
337 studies suggest there is an exponential relationship between ALWC and RH (e.g., Z. Wu et al., 2018).  
338 Here, we define the relative ALWC as the ratio of ALWC<sub>HTDMA</sub> and the function of ambient RH ( $e^{bRH}$ ).  
339 The b is derived according to the relationship between ALWC<sub>HTDMA</sub> and RH that is fitted by the  
340 function  $y = ae^{bx}$ . Figure 3a shows the relationship between relative ALWC and primary aerosols  
341 (PA) or SA mass concentrations. PA consists of primary organic aerosols (POA) and black carbon  
342 (BC), and SA consists of SOA, sulfate, and nitrate. The positive matrix factorization (Paatero and

343 Tapper, 1994) was applied on the organic aerosols (OA) spectral matrices to identify POA and SOA.  
344 The relative ALWC is highly correlated with SA mass concentrations ( $R^2 = 0.94$ ) but poorly correlated  
345 with PA mass concentrations ( $R^2 = 0.69$ ). High relative ALWCs coincident with high SA mass  
346 concentrations suggest that SA plays a key role in the increase in ALWC. This is likely because SA is  
347 mainly generated from photochemical reactions in the daytime or reactions at night, making SA highly  
348 aged with a hygroscopicity stronger than that of PA (Ervens et al., 2011; Sareen et al., 2017). SA can,  
349 therefore, absorb more water vapor than PA in the atmosphere. The enhanced aerosol liquid water  
350 induced by SA is further favorable for the formation of SA by speeding up the atmospheric chemical  
351 reaction rate and serving as the medium for gas-particle heterogeneous reactions (G. Wang et al., 2016;  
352 Cheng et al., 2016). This further increases the bulk aerosol hygroscopicity. This is also the reason why  
353 inferred  $\kappa$  based on the ZSR model continuously increases during haze episodes (Figure 2c).

354 Secondary aerosols are mainly composed of nitrate, sulfate, ammonium and SOA. To determine  
355 which species is the driver for ALWC in Beijing, Figure 3b shows the correlation analysis between  
356 relative ALWC and the mass concentrations of different aerosol chemical species. Relative ALWC and  
357 all SIA agree well [ $R^2$  equal to 0.66 (sulfate) and 0.56 (nitrate)]. It has been reported that ALWC is  
358 driven by inorganic salts with both nitrate and sulfate playing key roles in determining ALWC (Z. Wu  
359 et al., 2018). ALWC also agrees well with SOA ( $R^2 = 0.60$ ) in our study. This is unexpected because  
360 the hygroscopicity of SOA is relatively lower than that of nitrate and sulfate. Some studies have also  
361 suggested that the water uptake of aged organics accounts for only a few percent of the total aerosol  
362 water uptake (e.g., Gysel et al., 2007; Engelhart et al., 2011). In our study, the contribution of  $ALWC_{Org}$   
363 to total ALWC is significant, accounting for  $30\% \pm 22\%$ . As shown in Figure 4, the contribution of  
364 organics to total ALWC varies strongly. This is likely related with the variation in mass fraction and  
365 hygroscopicity parameter of organics ( $\kappa_{org}$ ). The mass concentration of inorganics increases more than  
366 that of organics as RH increases, leading to a lower mass fraction of organics in the case of high  
367 ambient RH. Figure 4 also shows  $ALWC_{Org}$  fraction increases significantly with the increase of  $\kappa_{org}$ .

368 All these help explain a large variation in the  $ALWC_{Org}$  contribution to total ALWC. Considering the  
369 distinct ambient RH and  $\kappa_{org}$  between clean and polluted periods, we calculated respectively the  
370 fraction of  $ALWC_{Org}$  during two periods. There is a higher  $ALWC_{Org}$  fraction ( $33\% \pm 23\%$ ) during  
371 clean periods than that during polluted periods ( $26\% \pm 11\%$ ). Yet, there is little variability of  $ALWC_{Org}$   
372 fraction during polluted periods. The larger variability in  $ALWC_{Org}$  fraction during clean periods is  
373 likely caused by the highly variable  $\kappa_{org}$  when the ambient RH is low. In summary, the contribution of  
374 organics in total ALWC varies with the variations of the mass fraction of organics and  $\kappa_{org}$ , and this  
375 contribution is significant during both clean and polluted periods. Studies of ALWC in Beijing,  
376 therefore, cannot neglect  $ALWC_{Org}$ . This is different from the studies in other regions such as in the  
377 Po Valley in Italy (Hodas et al., 2014) and the eastern U.S. (Carlton et al., 2013) where the ALWC was  
378 found to be only driven by nitrate and sulfate respectively.

379 An interesting phenomenon is frequently observed at the initial stage of heavy haze episodes (e.g.,  
380 P4, P5, P6, and P7).  $ALWC_{ISO}$  is almost close to 0, but both  $ALWC_{HTDMA}$  and  $ALWC_{Org}$  are always  
381 larger than 0, and the organic aerosol mass fraction is high at this stage. These observations reveal that  
382 at the initial stage of heavy haze episodes, the ALWC is mostly contributed by organic species.  
383 Meanwhile,  $\kappa$  is not very low and increases markedly as the  $PM_{10}$  mass concentration increases, which  
384 is unexpected because of the lower hygroscopicity of organic aerosols compared to SIA. Therefore,  
385 some highly hygroscopic substance (i.e., SA) must be generated through multiphase chemical reaction  
386 at this stage. We propose that the liquid water contributed by organic species provides a reactor for the  
387 transformation of gaseous precursors to SA at the initial stages of heavy haze episodes, increasing the  
388 uptake of more liquid water by more SA and further accelerating the formation of heavy haze. Section  
389 4.3 provides a case study to demonstrate this.

#### 390 **4.2.2. Impact of PNSD on ALWC**

391 In addition to aerosol chemical composition, ALWC also depends on PNSD (Bian et al., 2014).

392 [PNSD does not influence ALWC directly, but it's an important factor to determine the mass](#)

393 [concentration and the distribution of hygroscopic materials](#). As described in section 3.1, the nucleation  
394 mode (< 30 nm), the Aitken mode (30–110 nm), and the accumulation mode (110 nm to 1  $\mu$ m) (Whitby,  
395 1978; Birmili et al., 2001) are considered in this study. Particles with diameters greater than 1  $\mu$ m are  
396 not considered because some particles in the coarse mode are water soluble but their contribution on  
397 the ALWC is low (e.g., Hussein et al., 2004; S. Liu et al., 2008; Bian et al., 2014; Tan et al., 2017).

398 ~~Figure 5 shows that the~~ [The](#) contributions of nucleation mode, Aitken mode, and accumulation  
399 mode particles to  $ALWC_{HTDMA}$  are ~~about~~ 1.0 %, 18.0 %, and 82.0 %, respectively. Figure ~~6-5~~ shows  
400 the correlations between  $ALWC_{HTDMA}$  and the volume concentrations of different mode particles, and  
401 the average contribution of different mode particles to  $ALWC_{HTDMA}$  ( $f_{ALWC}$ ) under five different RH  
402 conditions. The  $R^2$  and  $f_{ALWC}$  of the nucleation mode particles (left column in Figure [65](#)) are all less  
403 than 0.1 and 1 %, respectively, under all RH conditions. This is likely because the volume  
404 concentration of nucleation mode particles is very low, and most of these small particles are composed  
405 of hydrophobic chemical species such as BC and POA. Similarly, the number concentration of Aitken  
406 mode particles also shows weak correlations with  $ALWC_{HTDMA}$  ( $R^2 < 0.2$ ) under  $RH < 90$  % conditions,  
407 but their correlation ( $R^2 = 0.25$ ) is enhanced significantly under  $RH > 90$  % conditions (middle column  
408 of Figure [65](#)). This is because there are more aged particles in the Aitken mode which can absorb much  
409 more water when the ambient RH is higher than 90 %. However, the contribution of the Aitken mode  
410 to ALWC ranges from 14 % to 21 % and decreases as RH increases.  $ALWC_{HTDMA}$  is strongly correlated  
411 to the volume concentration of accumulation mode particles, with  $R^2$  and  $f_{ALWC}$  greater than 0.6 and  
412 75 %, respectively, under all RH conditions (right column of Figure [65](#)). Figure ~~6-5~~ also shows that  
413 ALWC increases slightly as the volume concentration of accumulation mode particles increases under  
414  $RH < 70$  % conditions (slope < 0.001), but increases strongly under higher RH conditions, especially  
415 under  $RH > 90$  % conditions (slope = 0.0041). This is likely because there are more accumulation  
416 mode SA formed due to multiphase chemical reactions under high ambient RH conditions. Swietlicki  
417 et al. (1999) have suggested that the contribution of accumulation mode particles to ALWC is largest



418 for all-mode particles.

419 In summary, the contribution of nucleation mode particles to ALWC is very low. The contribution  
420 of Aitken mode particles is much higher than nucleation mode particles and decreases with increasing  
421 ambient RH. The contribution of accumulation mode particles to ALWC is largest under all RH  
422 conditions and increases with increasing ambient RH, thus playing a key role in determining ALWC.

#### 423 4.2.3. Impact of RH on ALWC

424 As discussed in 4.2.1, the absolute value of ALWC has an exponential relationship with ambient  
425 RH. Figure 7-6 shows the relationship between ALWC and RH for different PM<sub>1</sub> mass concentration  
426 ranges. ALWC increases slowly as RH increases under lower ambient RH conditions then sharply  
427 increases when RH exceeds a critical RH value. This critical RH value is different for different PM<sub>1</sub>  
428 mass concentrations. This is because the low RH conditions cannot provide enough water for aerosol  
429 particles, even though the PNSD is dominated by accumulation mode particles with higher  
430 hygroscopicity (Tan et al., 2016). This demonstrates the important influence of RH on ALWC. The  
431 lower critical RH value for higher PM<sub>1</sub> mass concentrations (~80 %) suggests that ALWC is easily  
432 formed under heavily polluted conditions. This is likely because there are more SA and accumulation  
433 mode particles during pollution periods (Sun et al., 2016a; Y. Wang et al., 2017).

434 Figure 8a-7a shows the diurnal variations of ALWC<sub>HTDMA</sub> and ambient RH during the sampling  
435 period. The extreme ALWC<sub>HTDMA</sub> values appear at night and during the day respectively, likely related  
436 to the diurnal variations of ambient RH. The elevated ambient RH at night not only increases ALWC  
437 through water uptake of particles directly, but also facilitates the formation of hydrophilic particulate  
438 nitrate through the speeding up of the uptake coefficient of N<sub>2</sub>O<sub>5</sub> (Thornton et al., 2003; Bertram et  
439 al., 2009). This can further enhance ALWC. However, although the diurnal variations of ALWC<sub>HTDMA</sub>  
440 and ambient RH are similar, the peak and nadir of ALWC<sub>HTDMA</sub> (0300 LT and 1100 LT, respectively)  
441 appear three hours earlier than the peak and nadir of ambient RH (0600 LT and 1400 LT, respectively).  
442 This time difference is likely related to changes in PNSD. The diurnal variation of PNSD (Figure 8b-7b)

443 shows that the number concentrations of Aitken and accumulation mode particles begin to decrease  
444 quickly at 0300 LT. ALWC also begins to decrease, although the ambient RH increases slightly at that  
445 time. In the morning, ALWC decreases sharply following the ambient RH and PNSD changes due to  
446 the lifting planetary boundary layer height. ALWC decreases to its minimum value at ~1100 LT then  
447 begins to increase quickly. However, ambient RH still decreases at that time and reaches its minimum  
448 value at ~1400 LT. The increase in ALWC is likely associated with changes in aerosol chemical species  
449 and PNSD. Figure 8b-7b and 8e-7c show that there are many newly formed Aitken and accumulation  
450 mode particles and that the fraction of SA increases at noon, likely because of strong photochemical  
451 reactions. Y. Wang et al. (2017, 2018) have suggested that daytime photochemical reactions are  
452 efficient enough to enhance aerosol hygroscopicity and change the aerosol mixing state from external  
453 to internal in North China through the formation of hydrophilic chemical species. All this suggests that  
454 ambient RH is not the only determining factor for ALWC. PNSD and aerosol chemical composition  
455 are also important for ALWC.

#### 456 4.3. A case study of the impact of $ALWC_{Org}$ on SA formation

457 As discussed in section 4.2.1, a hypothesis is proposed that  $ALWC_{Org}$  maybe provide a reactor for  
458 the formation of secondary species. To verify this hypothesis, the P4 case shown in Figure2 is selected  
459 to further analyze the influence of  $ALWC_{Org}$  on the formation of secondary aerosols (Figure 98). Figure  
460 9a-8a shows the time series of  $ALWC_{HTDMA}$ ,  $ALWC_{ISO}$ , and  $ALWC_{Org}$  during this case. On 27  
461 November 2017,  $ALWC_{ISO}$  was close to 0 all day long because of the low ambient RH, but both  
462  $ALWC_{HTDMA}$  and  $ALWC_{Org}$  were always larger than 0, increasing with increasing  $PM_{10}$  mass  
463 concentration (Figure 9a8a). Figure 9a-8a also shows that the fraction of  $ALWC_{Org}$  in  $ALWC_{HTDMA}$   
464 was high at the initial stage of this pollution case, but this fraction decreased as haze increased. This  
465 case was further divided into three periods (Figure 9b8b). Organics were the most abundant chemical  
466 species during the first period (64 %), which explains the high fraction of  $ALWC_{Org}$  in  $ALWC_{HTDMA}$  at  
467 the initial stage of this haze case. The pie charts in Figure 9b-8b also show that both SOA and SIA

468 (sulfate, nitrate, and ammonium) increases from the first to third periods but POA decreases, likely  
469 related to multiphase reactions (i.e., aqueous-phase reactions) due to the enhanced ALWC. Time series  
470 of  $f_{44}$  and the fraction of sulfate in total sulfur ( $F_{\text{SO}_4^{2-}}$ ) are also shown to further illustrate the influence  
471 of aqueous-phase reactions on aerosol chemical species. The  $m/z$  44 signal intensity  $f_{44}$  (mostly  
472 contributed by the  $\text{CO}_2^+$  ion) measured by the AMS can be used as an indicator of the oxidation level  
473 in organic species (Mei et al., 2013). The sulfur oxidation ratio  $F_{\text{SO}_4^{2-}}$  (Sun et al., 2006) is defined as

$$474 \quad F_{\text{SO}_4^{2-}} = \frac{n[\text{SO}_4^{2-}]}{n[\text{SO}_4^{2-}] + n[\text{SO}_2]}, \quad (10)$$

475 where  $n[\text{SO}_4^{2-}]$  and  $n[\text{SO}_2]$  refer to the molar concentrations of  $\text{SO}_4^{2-}$  and  $\text{SO}_2$ , respectively. Figure 9b  
476 8b suggests that  $f_{44}$  and  $F_{\text{SO}_4^{2-}}$  both increase gradually with increasing  $\text{ALWC}_{\text{HTDMA}}$  and  $\text{PM}_{10}$  mass  
477 concentration from 27 November to 30 November 2017. This is likely because the increase in ALWC  
478 is beneficial to the oxidation of organics and the transformation of  $\text{SO}_2$  to  $\text{SO}_4^{2-}$ , implying the  
479 importance of aqueous-phase chemical reaction on haze formation in Beijing. The production of  
480 secondary organic and inorganic species can further enhance aerosol hygroscopicity, increasing ALWC  
481 in the atmosphere. This positive feedback is the reason behind the rapid formation of heavy haze events  
482 in Beijing (G. Wang et al., 2016). A rapid increase in  $f_{44}$  and  $F_{\text{SO}_4^{2-}}$  was seen during the first period at  
483 night on 27 November (shown by green and red arrows in Fig. 9) when organics contributed the most  
484 to ALWC. This suggests that ALWC contributed by organics may have played an important role in the  
485 formation of secondary species at the initial stage of the pollution event.

486

## 487 5. Conclusions

488 In this study, the aerosol liquid water content (ALWC) was calculated using the size-resolved  
489 aerosol hygroscopic growth factor and the particle number size distribution (PNSD) measured at a  
490 Beijing urban site during the APHH winter campaign (8 November to 15 December 2017). Also done

491 were simulations using the ISORROPIA II model with measured aerosol chemical composition data  
492 as input data. During the sampling period, seven heavy haze episodes were selected to investigate the  
493 influence of different factors (PNSD, ambient RH, and aerosol chemical composition) on ALWC.

494 The calculated and simulated ALWC ( $ALWC_{HTDMA}$  and  $ALWC_{ISO}$ ) agree well (correlation of  
495 determination  $R^2$  equal to 0.89). However,  $ALWC_{ISO}$  is much lower than  $ALWC_{HTDMA}$  for RH below  
496 60 %, even approaching zero many times. This deviation is in part attributed to the neglect of the  
497 contribution of organics to ALWC ( $ALWC_{Org}$ ) in the ISORROPIA II model, contradicting with  
498 previous studies ignoring this contribution. The aerosol hygroscopicity of organics was also derived  
499 in this study for use in calculating  $ALWC_{Org}$ . The sum of  $ALWC_{ISO}$  and  $ALWC_{Org}$  has a higher  
500 correlation ( $R^2 = 0.92$ ) with the calculated ALWC (i.e.,  $ALWC_{HTDMA}$ ), especially for RH below 60 %.  
501 This implies that organic aerosols are also an important contributor to ALWC.

502 PNSD, ambient RH, and aerosol chemical composition are all found to affect ALWC significantly.  
503 Nucleation mode and Aitken mode particles have little influence on ALWC. Accumulation mode  
504 particles play a key role in determining ALWC and dominate among all aerosol modes. ALWC is  
505 highly related to the relative humidity (RH) when RH exceeds a critical RH value that is different for  
506 different  $PM_{10}$  mass concentrations. ALWC varies diurnally with its extreme values appearing at night  
507 and during the day respectively. The diurnal variation of ambient RH explains this. However, there is  
508 a three-hour difference between when the extreme ALWC and RH values occur, caused by the diurnal  
509 variations in PNSD and aerosol chemical composition.

510 On average,  $ALWC_{Org}$  accounts for  $\sim 30 \% \pm 22 \%$  of the total aerosol liquid water during the  
511 sampling period. This shows the significant contribution of organic species to ALWC. Our results  
512 suggest that ALWC is not only driven by inorganic salts but also driven by organics in Beijing. This is  
513 different from the results obtained in the Po Valley in Italy (Hodas et al., 2014) and the eastern U.S.  
514 (Carlton et al., 2013) where the ALWC is driven by nitrate and sulfate respectively. Finally, one case  
515 study was used to study the importance of  $ALWC_{Org}$  on multiphase chemical reactions.  $ALWC_{Org}$  was

516 found to play an important role in the formation of secondary aerosols by speeding up aqueous-phase  
517 reactions at the initial stage of heavy haze. Our study is important for investigating the contribution of  
518 organics to ALWC and its importance on haze formation in Beijing.

519

520 *Data availability.* Data used in the study are available from the first author upon request

521 ([201631490012@mali.bnu.edu.cn](mailto:201631490012@mali.bnu.edu.cn)).

522

523 *Author contributions.* ZL and YW designed the experiment; YW, XJ, and WX carried it out and  
524 analyzed the data; other co-authors participated in science discussions and suggested additional  
525 analyses. XJ and YW prepared the paper with contributions from all co-authors.

526

527 *Competing interests.* The authors declare no competing interests.

528

529 *Acknowledgements.* This work was funded by the National Key R&D Program of China (grant no.  
530 2017YFC1501702), the National Natural Science Foundation of China (NSFC) research projects  
531 (grant nos. 91544217, 41575132, 41675141, 41705125), the Startup Foundation for Introducing Talent  
532 of NUIST ([grant no. 2019r077](#)), and the National Basic Research Program of China “973” (grant no.  
533 2013CB955801). We thank all participants of the field campaign for their tireless work and  
534 cooperation.

535

## 536 **References**

537

538 Abbatt, J. P. D., Lee, A. K. Y., Thornton, J. A.: Quantifying Trace Gas Uptake to Tropospheric Aerosol:  
539 Recent Advances and Remaining Challenges, *Chem. Soc. Rev.*, 41(19), 6555–6581,  
540 <https://doi.org/10.1039/c2cs35052a>, 2012.

541 Adams, P. J., and Seinfeld, J. H.: General circulation model assessment of direct radiative forcing by  
542 the sulfate-nitrate-ammonium-water inorganic aerosol system, *J. Geophys. Res.-Atmos.*, 106,

带格式的: 字体: (默认) Times New Roman, (中文) 宋体,  
小四, 字体颜色: 文字 1, 图案: 清除

带格式的: 字体: (中文) 宋体, 字体颜色: 文字 1

1097–1111, <https://doi.org/10.1029/2000JD900512>, 2001.

544 Ansari, A.S., Pandis, S.N.: Prediction of multicomponent inorganic atmospheric aerosol behavior,  
545 *Atmos. Environ.*, 33 (5), 745–757, [https://doi.org/10.1016/S1352-2310\(98\)00221-0](https://doi.org/10.1016/S1352-2310(98)00221-0), 1999.

546 Arellanes, C., Paulson, S. E., Fine, P. M., and Sioutas, C.: Exceeding of Henry’s Law by Hydrogen  
547 Peroxide Associated with Urban Aerosols, *Environ. Sci. Technol.*, 40, 4859–4866,  
548 <https://doi.org/10.1021/es0513786>, 2006.

549 Bertram, T. H., Thornton, J. A.: Toward a general parameterization of N<sub>2</sub>O<sub>5</sub> reactivity on aqueous  
550 particles: the competing effects of particle liquid water, nitrate and chloride, *Atmos. Chem. Phys.*, 9  
551 (21), 8351–8363, <https://doi.org/10.5194/acp-9-8351-2009>, 2009.

552 Bian, Y.X., Zhao, C.S., Ma, N., Chen, J., Xu, W.Y.: A study of aerosol liquid water content based on  
553 hygroscopicity measurements at high relative humidity in the North China Plain, *Atmos. Chem.  
554 Phys.*, 14 (12), 6417–6426, <https://doi.org/10.5194/acp-14-6417-2014>, 2014.

555 Birmili, W., Wiedensohler, A., Heintzenberg, J., and Lehmann, K.: Atmospheric particle number size  
556 distribution in central Europe: Statistical relations to air masses and meteorology, *J. Geophys. Res.-  
557 Atmos.*, 106, 32005–32018, <https://doi.org/10.1029/2000JD000220>, 2001.

558 Blando, J. D., Turpin, B. J.: Secondary organic aerosol formation in cloud and fog droplets: a literature  
559 evaluation of plausibility, *Atmos. Environ.*, 34, 1623–1632, [https://doi.org/10.1016/S1352-  
560 2310\(99\)00392-1](https://doi.org/10.1016/S1352-2310(99)00392-1), 2001.

561 Carbone, S., Saarikoski, S., Frey, A., Reyes, F., Reyes, P., Castillo, M., Gramsch, E., Oyola, P., Jayne,  
562 J., Worsnop, DR., and Hillamo, R.: Chemical characterization of submicron aerosol particles in  
563 Santiago de Chile, *Aerosol Air Qual. Res.*, 13(2), 462–473,  
564 <https://doi.org/10.4209/aaqr.2012.10.0261>, 2013.

565 Carlton, A. G., Turpin, B. J.: Particle partitioning potential of organic compounds is highest in the  
566 Eastern US and driven by anthropogenic water, *Atmos. Chem. Phys.*, 13 (20), 10203–10214,  
567 <https://doi.org/10.5194/acp-13-10203-2013>, 2013.

568 Cerully, K. M., Bougiatioti, A., Hite Jr., J. R., Guo, H., Xu, L., Ng, N. L., Weber, R., and Nenes, A.:  
569 On the link between hygroscopicity, volatility, and oxidation state of ambient and water-soluble  
570 aerosol in the Southeastern United States, *Atmos. Chem. Phys.*, 14, 30835–30877,  
571 <https://doi.org/10.5194/acpd-14-30835-2014>, 2014.

572 Chen, J., Zhao, C. S., Ma, N., Liu, P. F., Göbel, T., Hallbauer, E., Deng, Z. Z., Ran, L., Xu, W. Y.,  
573 Liang, Z., Liu, H. J., Yan, P., Zhou, X. J., and Wiedensohler, A.: A parameterization of low visibilities  
574 for hazy days in the North China Plain, *Atmos. Chem. Phys.*, 12, 4935–4950,  
575 <https://doi.org/10.5194/acp-12-4935-2012>, 2012.

576 Cheng, Y., Zheng, G., Wei, C., Mu, Q., Zheng, B., Wang, Z., Gao, M., Zhang, Q., He, K., Carmichael,

577 G., Pöschl, U., Su, H.: Reactive nitrogen chemistry in aerosol water as a source of sulfate during  
578 haze events in China, *Sci. Adv.*, 2 (12), e1601530, <https://doi.org/10.1126/sciadv.1601530>, 2016.

579 Dougle, P. G., Vlasenko, A. L., Veefkind, J. P., and Brink, H. M. T.: Humidity dependence of the light  
580 scattering by mixtures of ammonium nitrate, ammonium sulfate and soot, *J. Aerosol. Sci.*, 27, 513–  
581 514, [https://doi.org/10.1016/0021-8502\(96\)00329-1](https://doi.org/10.1016/0021-8502(96)00329-1), 1996.

582 Engelhart, G.J., Hildebrandt, L., Kostenidou, E., Mihalopoulos, N., Donahue, N.M., Pandis, S.N.:  
583 Water content of aged aerosol, *Atmos. Chem. Phys.*, 11, 911–920, <https://doi.org/10.5194/acp-11-911-2011>, 2011.

584

585 Ervens, B., Turpin, B. J., Weber, R. J.: Secondary organic aerosol formation in cloud droplets and  
586 aqueous particles (aqSOA): a review of laboratory, field and model studies, *Atmos. Chem. Phys.*,  
587 11 (21), 11069–11102, <https://doi.org/10.5194/acp-11-11069-2011>, 2011.

588 Fountoukis, C. and Nenes, A.: ISORROPIA II: a computationally efficient thermodynamic equilibrium  
589 model for  $K^+$ – $Ca^{2+}$ – $Mg^{2+}$ – $NH_4^+$ – $Na^+$ –SONO– $Cl^-$ – $H_2O$  aerosols, *Atmos. Chem. Phys.*, 7, 4639–  
590 4659, <https://doi.org/10.5194/acp-7-4639-2007>, 2007.

591 Gao, Y., Liu, X., Zhao, C., and Zhang, M.: Emission controls versus meteorological conditions in  
592 determining aerosol concentrations in Beijing during the 2008 Olympic Games, *Atmos. Chem.*  
593 *Phys.*, 11, 12437–12451, <https://doi.org/10.5194/acp-11-12437-2011>, 2011.

594 Gysel, M., Grosier, J., Topping, D.O., Whitehead, J.D., Bower, J.N., Cubison, M.J., Williams, P.I.,  
595 Flynn, M.J., McFiggans, G.B., Coe, H.: Closure study between chemical composition and  
596 hygroscopic growth of aerosol particles during TORCH2, *Atmos. Chem. Phys.*, 7 (24), 6131–6144,  
597 <https://doi.org/10.5194/acp-7-6131-2007>, 2007.

598 Hennigan, C. J., Bergin, M. H., Dibb, J. E., Weber, R. J.: Enhanced secondary organic aerosol  
599 formation due to water uptake by fine particles, *Geophys. Res. Lett.*, 35(18), No. L18801,  
600 <https://doi.org/10.1029/2008GL035046>, 2008.

601 Hodas, N., Sullivan, A. P., Skog, K., Keutsch, F. N., Collett, J. L., Decesari, S., Facchini, M. C.,  
602 Carlton, A. G., Laaksonen, A., Turpin, B. J.: Aerosol Liquid Water Driven by Anthropogenic Nitrate:  
603 Implications for Lifetimes of Water-Soluble Organic Gases and Potential for Secondary Organic  
604 Aerosol Formation, *Environ. Sci. Technol.*, 48 (19), 11127–11136  
605 <https://doi.org/10.1021/es5025096>, 2014.

606 Huang, R., Zhang, Y., Bozzetti, C., Ho, K., Cao, J., Han, Y., Daellenbach, K. R., Slowik, J. G., Platt,  
607 S. M., Canonaco, F.: High secondary aerosol contribution to particulate pollution during haze events  
608 in China, *Nature.*, 514 (7521), 218, <https://doi.org/10.1038/nature13774>, 2014.,

609 Hussein, T., Puustinen, A., Aalto, P. P., Mäkelä, J. M., Hämeri, K., and Kulmala, M.: Urban aerosol

610 number size distributions, *Atmos. Chem. Phys.*, 4, 391–411, <https://doi.org/10.5194/acp-4-391->  
611 2004, 2004.

612 Hussein, T., Dal Maso, M., Petäjä, T., Koponen, I. K., Paatero, P., Aalto, P. P., Hämeri, K., and Kulmala,  
613 M.: Evaluation of an automatic algorithm for fitting the particle number size distributions, *Boreal*  
614 *Environ. Res.*, 10, 337–355, 2005.

615 Jimenez, J. L., Jayne, J. T., Shi, Q., Kolb, C. E., Worsnop, D. R., Yourshaw, I., Morris, J. W.: Ambient  
616 aerosol sampling using the aerodyne aerosol mass spectrometer, *J. Geophys. Res.-Atmos.*, 108(D7),  
617 <https://doi.org/https://doi.org/10.1029/2001JD001213>, 2003.

618 Kim, Y.P., Seinfeld, J.H., Saxena, P.: Atmospheric gas-aerosol equilibrium I. Thermodynamic model,  
619 *Aerosol Sci. Technol.*, 19 (2), 157–181, <https://doi.org/10.1080/02786829308959628>, 1993.

620 Kitamori, Y., Mochida, M., Kawamura, K.: Assessment of the aerosol water content in urban  
621 atmospheric particles by the hygroscopic growth measurements in Sapporo, Japan. *Atmos. Environ.*,  
622 43 (21), 3416–3423, <https://doi.org/10.1016/j.atmosenv.2009.03.037>, 2009.

623 Kuang Y., Zhao C.S., Ma N., Liu H.J., Bian Y.X., Tao J.C. and Hu M.: Deliquescent phenomena of  
624 ambient aerosols on the North China Plain, *Geophys Res Lett*, 43, 8744-8750,  
625 <https://doi.org/10.1002/2016GL070273>, 2016.

626 Kuang, Y., Zhao, C. S., Zhao, G., Tao, J. C., Xu, W., Ma, N., and Bian, Y. X.: A novel method for  
627 calculating ambient aerosol liquid water content based on measurements of a humidified  
628 nephelometer system, *Atmospheric Measurement Techniques*, 11(5), 2967-2982,  
629 <https://doi.org/10.5194/amt-11-2967-2018>, 2018.

630 Latham, T. L., Beyersdorf, A. J., Thornhill, K. L., Winstead, E. L., Cubison, M. J., Hecobian, A.,  
631 Jimenez, J. L., Weber, R. J., Anderson, B. E., and Nenes, A.: Analysis of CCN activity of Arctic  
632 aerosol and Canadian biomass burning during summer 2008, *Atmos. Chem. Phys.*, 13, 2735–2756,  
633 <https://doi.org/10.5194/acp-13-2735-2013>, 2013.

634 Liao, H., Seinfeld, J. H.: Global impacts of gas-phase chemistry aerosol interactions on direct radiative  
635 forcing by anthropogenic aerosols and ozone, *J. Geophys. Res.-Atmos.*, 110 (D18).  
636 <https://doi.org/10.1029/2005JD005907>, 2005.

637 Li, Z., Lau, W. M., Ramanathan, V., Wu, G., Ding, Y., Manoj, M. G., Liu, J., Qian, Y., Li, J., and Zhou,  
638 T.: Aerosol and monsoon climate interactions over Asia, *Rev. Geophys.*, 54, 866–929,  
639 <https://doi.org/10.1002/2015RG000500>, 2016.

640 Liu, S., Hu, M., Wu, Z., Wehner, B., Wiedensohler, A., and Cheng, Y.: Aerosol number size distribution  
641 and new particle formation at a rural/coastal site in Pearl River Delta (PRD) of China, *Atmos.*  
642 *Environ.*, 42, 6275–6283, <https://doi.org/10.1016/j.atmosenv.2008.01.063>, 2008.

643 Mei F., Setyan A., Zhang Q. and Wang J.: CCN activity of organic aerosols observed downwind of



644 urban emissions during CARES, *Atmos. Chem. Phys.*, 13, 12155-12169,  
645 <https://doi.org/10.5194/acp-13-12155-2013>, 2013.

646 Moore, R. H., Bahreini, R., Brock, C. A., Froyd, K. D., Cozic, J., Holloway, J. S., Middlebrook, A. M.,  
647 Murphy, D. M., and Nenes, A.: Hygroscopicity and composition of Alaskan Arctic CCN during  
648 April 2008, *Atmos. Chem. Phys.*, 11, 11807–11825, <https://doi.org/10.5194/acp-11-11807-2011>,  
649 2011.

650 Nenes, A., Pandis, S.N., Pilinis, C.: ISORROPIA: a new thermodynamic equilibrium model for  
651 multiphase multicomponent inorganic aerosols, *Aquat. Geochem.*, 4 (1), 123–152,  
652 <https://doi.org/10.1023/A:1009604003981>, 1998.

653 Nguyen, T. K. V., Zhang, Q., Jimenez, J. L., Pike, M., Carlton, A. G.: Liquid Water: Ubiquitous  
654 Contributor to Aerosol Mass, *Environ. Sci. Technol. Lett.*, 3 (7), 257–263,  
655 <https://doi.org/10.1021/acs.estlett.6b00167>, 2016.

656 Paatero, P., & Tapper, U. (2010). Positive matrix factorization: a non-negative factor model with  
657 optimal utilization of error estimates of data values. *Environmetrics*, 5(2), 111-126.

658 Petters, M. D. and Kreidenweis, S. M.: A single parameter representation of hygroscopic growth and  
659 cloud condensation nucleus activity, *Atmos. Chem. Phys.*, 7, 1961–1971,  
660 <https://doi.org/10.5194/acp-7-1961-2007>, 2007.

661 Sareen, N., Waxman, E. M., Turpin, B. J., Volkamer, R., Carlton, A. G.: Potential of Aerosol Liquid  
662 Water to Facilitate Organic Aerosol Formation: Assessing Knowledge Gaps about Precursors and  
663 Partitioning, *Environ. Sci. Technol.*, 51 (6), 3327–3335, <https://doi.org/10.1021/acs.est.6b04540>,  
664 2017.

665 Seinfeld, H. J., Pandis, N. S.: *Atmospheric Chemistry and Physics: From Air Pollution to Climate*  
666 *Change*, Taylor & Francis Group, <https://doi.org/10.1080/00139157.1999.10544295>, 2006.

667 Sjogren, S., Gysel, M., Weingartner, E., Baltensperger, U., Cubison, M. J., Coe, H., Zardini, A. A.,  
668 Marcolli, C., Krieger, U. K., and Peter, T.: Hygroscopic growth and water uptake kinetics of two-  
669 phase aerosol particles consisting of ammonium sulfate, adipic and humic acid mixtures, *J. Aerosol*  
670 *Sci.*, 38, 157–171, <https://doi.org/10.1016/j.jaerosci.2006.11.005>, 2007.

671 Song, S., Gao, M., Xu, W., et al.: Possible heterogeneous chemistry of hydroxyl-methane-sulfonate  
672 (HMS) in northern China winter haze, *Atmos. Chem. Phys.*, 19(2): 1357-1371,  
673 <https://doi.org/10.5194/acp-19-1357-2019>, 2019.

674 Stanier, C.O., Khlystov, A.Y., Chan, W.R., Mandiro, M., Pandis, S.N.: A method for the in situ  
675 measurement of fine aerosol water content of ambient aerosols: The Dry Ambient Aerosol Size  
676 Spectrometer (DAASS), *Aerosol Sci. Technol.*, 38 (1), 215–228,  
677 <https://doi.org/10.1080/02786820390229525>, 2004.

678 Stokes, R. H. and Robinson, R. A.: Interactions in aqueous nonelectrolyte solutions. I. Solute-solvent  
679 equilibria, *J. Phys. Chem.*, 70, 2126–2131, <https://doi.org/10.1021/j100879a010>, 1966.

680 Sun, Y., Zhuang, G., Tang, A., Wang, Y., An, Z.: Chemical characteristics of PM<sub>2.5</sub> and PM<sub>10</sub> in haze-  
681 fog episodes in Beijing, *Environ. Sci. Technol.*, 40, 3148–3155, <https://doi.org/10.1021/es051533g>,  
682 2006.

683 Sun, Y., Z. F. Wang, P. Q. Fu, T. Yang, Q. Jiang, H. B. Dong, J. Li, and J. J. Jia.: Aerosol composition,  
684 sources and processes during wintertime in Beijing, China, *Atmos. Chem. Phys.*, 13(9), 4577–4592,  
685 <https://doi.org/10.5194/acp-13-4577-2013>, 2013.

686 Sun Y., Chen C., Zhang Y., Xu W., Zhou L., Cheng X., Zheng H., Ji D., Jie L. and Xiao T.: Rapid  
687 formation and evolution of an extreme haze episode in Northern China during winter 2015, *Sci.*  
688 *Rep.*, 6(1):27151, <https://doi.org/10.1038/srep27151>, 2016a.

689 Sun, Y., Wang, Z., Wild, O., Xu, W., Chen, C., Fu, P., Du, W., Zhou, L., Zhang, Q., and Han, T.: “APEC  
690 Blue”: Secondary Aerosol Reductions from Emission Controls in Beijing, *Sci. Rep.*, 6, 20668,  
691 <https://doi.org/10.1038/srep20668>, 2016b.

692 Surratt, J. D., Kroll, J. H., Kleindienst, T. E., Edney, E. O., Claeys, M., Sorooshian, A., Ng, N. L.,  
693 Offenberg, J. H., Lewandowski, M., Jaoui, M., Flagan, R. C., Seinfeld, J. H.: Evidence for  
694 organosulfates in secondary organic aerosol, *Environ. Sci. Technol.*, 41, 517–527,  
695 <https://doi.org/10.1021/es062081q>, 2007.

696 Swietlicki, E., Zhou, J., Berg, O. H., Martinsson, B. G., Frank, G., Cederfelt, S. I., Dusek, U., Berner,  
697 A., Birmili, W., Wiedensohler, A., Yuskiewicz, B., and Bower, K. N.: A closure study of sub-  
698 micrometer aerosol particle hygroscopic behaviour, *Atmos. Res.*, 50, 205–240,  
699 [https://doi.org/10.1016/S0169-8095\(98\)00105-7](https://doi.org/10.1016/S0169-8095(98)00105-7), 1999.

700 Tan, H., Cai, M., Fan, Q., Liu, L., Li, F., & Chan, P. W., et al.: An analysis of aerosol liquid water  
701 content and related impact factors in pearl river delta, *Science of The Total Environment*, 579, 1822-  
702 1830, <https://doi.org/10.1016/j.scitotenv.2016.11.167>, 2017.

703 Tao, W. K., Chen, J. P., Li, Z., Wang, C., and Zhang, C.: Impact of Aerosols on Convective Clouds and  
704 Precipitation, *Rev. Geo. phys.*, 50, 1–62, <https://doi.org/10.1029/2011RG000369>, 2012.

705 Thornton, J. A., Braban, C. F., Abbatt, J. P. D.: N<sub>2</sub>O<sub>5</sub> hydrolysis on sub-micron organic aerosols: the  
706 effect of relative humidity, particle phase, and particle size. *Atmos. Chem. Phys.*, 5 (20), 4593–4603,  
707 <https://doi.org/10.1039/b307498f>, 2003.

708 Topping D O, Mcfiggans G B, Coe H.: A curved multi-component aerosol hygroscopicity model  
709 framework: Part 1 – Inorganic compounds, *Atmos. Chem. Phys.*, 5(5): 1205-1222,  
710 <https://doi.org/10.5194/acp-5-1205-2005>, 2005.

711 Wahner, A., Mentel, T. F., Sohn, M., Stier, J.: Heterogeneous reaction of N<sub>2</sub>O<sub>5</sub> on sodium nitrate  
712 aerosol, *J. Geophys. Res. Atmos*, 103 (D23), 31103–31112, <https://doi.org/10.1029/1998JD100022>,  
713 1998.

714 Wang, G., Zhang, R., Gomez, M. E., Yang, L., Levy Zamora, M., Hu, M., Lin, Y., Peng, J., Guo, S.,  
715 Meng, J., Li, J., Cheng, C., Hu, T., Ren, Y., Wang, Y., Gao, J., Cao, J., An, Z., Zhou, W., Li, G.,  
716 Wang, J., Tian, P., MarreroOrtiz, W., Secretst, J., Du, Z., Zheng, J., Shang, D., Zeng, L., Shao, M.,  
717 Wang, W., Huang, Y., Wang, Y., Zhu, Y., Li, Y., Hu, J., Pan, B., Cai, L., Cheng, Y., Ji, Y., Zhang, F.,  
718 Rosenfeld, D., Liss, P. S., Duce, R. A., Kolb, C. E., Molina, M. J.: Persistent sulfate formation from  
719 London Fog to Chinese haze, *Proc. Natl. Acad. Sci. U. S. A.*, 113 (48), 13630–13635,  
720 <https://doi.org/10.1073/pnas.1616540113>, 2016.

721 Wang, H., Lu, K., Chen, X., Zhu, Q., Chen, Q., Guo, S., Jiang, M., Li, X., Shang, D., Tan, Z., Wu, Y.,  
722 Wu, Z., Zou, Q., Zheng, Y., Zeng, L., Zhu, T., Hu, M., Zhang, Y.: High N<sub>2</sub>O<sub>5</sub> Concentrations  
723 Observed in Urban Beijing: Implications of a Large Nitrate Formation Pathway, *Environ. Sci.*  
724 *Technol. Lett.*, 4 (10), 416–420, <https://doi.org/10.1021/acs.estlett.7b00341>, 2017.

725 Wang, T., Nie, W., Gao, J., Xue, L. K., Gao, X. M., Wang, X. F., Qiu, J., Poon, C. N., Meinardi, S.,  
726 Blake, D., Wang, S. L., Ding, A. J., Chai, F. H., Zhang, Q. Z., and Wang, W. X.: Air quality during  
727 the 2008 Beijing Olympics: secondary pollutants and regional impact, *Atmos. Chem. Phys.*, 10,  
728 7603–7615, <https://doi.org/10.5194/acp-10-7603-2010>, 2010.

729 Wang, Y., Zhang, Q., Jiang, J., Zhou, W., Wang, B., He, K., Duan, F., Zhang, Q., Philip, S., and Xie,  
730 Y.: Enhanced sulfate formation during China’s severe winter haze episode in January 2013 missing  
731 from current models, *J. Geophys. Res.-Atmos.*, 119, 10425–10440,  
732 <https://doi.org/10.1002/2013JD021426>, 2014.

733 Wang Y., Zhang F., Li Z., Tan H., Xu H., Ren J., Zhao J., Du W. and Sun Y.: Enhanced hydrophobicity  
734 and volatility of submicron aerosols under severe emission control conditions in Beijing, *Atmos*  
735 *Chem Phys*, 17, 5239-5251, <https://doi.org/10.5194/acp-17-5239-2017>, 2017.

736 Wang Y., Li Z., Zhang Y., Du W., Zhang F., Tan H., Xu H., Fan T., Jin X., Fan X., Dong Z., Wang Q.  
737 and Sun Y.: Characterization of aerosol hygroscopicity, mixing state, and CCN activity at a suburban  
738 site in the central North China Plain, *Atmos. Chem. Phys.*, 18, 11739-11752,  
739 <https://doi.org/10.5194/acp-18-11739-2018>, 2018.

740 Wehner, B., Birmili, W., Ditas, F., Wu, Z., Hu, M., Liu, X., Mao, J., Sugimoto, N., and Wiedensohler,  
741 A.: Relationships between sub micrometer particulate air pollution and air mass history in Beijing,  
742 China, 2004–2006, *Atmos. Chem. Phys.*, 8, 6155–6168, <https://doi.org/10.5194/acp-8-6155-2008>,  
743 2008.

744 [Wei, J., Huang, W., Li, Z., Xue, W., Peng, Y., Sun, L., and Cribb, M. Estimating 1-km-resolution PM<sub>2.5</sub>](#)

745 [concentrations across China using the space-time random forest approach. \*Remote Sensing of\*](#)  
746 [Environment](#), 231, 1-14. <https://doi.org/10.1016/j.rse.2019.111221>, 2019a.

747 [Wei, J., Li, Z., Guo, J., Sun, L., Huang, W., Xue, W., Fan, T., and Cribb, M. Satellite-derived 1-km-](#)  
748 [resolution PM<sub>1</sub> concentrations from 2014 to 2018 across China. \*Environmental Science &\*](#)  
749 [Technology](#). <https://doi.org/10.1021/acs.est.9b03258>, 2019b.

750 Wexler, A.S., Clegg, S.L.: Atmospheric aerosol models for systems including the ions H<sup>+</sup>, NH<sub>4</sub><sup>+</sup>, Na<sup>+</sup>,  
751 SO<sub>4</sub><sup>2-</sup>, NO<sub>3</sub><sup>-</sup>, Cl<sup>-</sup>, Br<sup>-</sup>, and H<sub>2</sub>O, *J. Geophys. Res.-Atmos.*, 107 (D14): 14-14,  
752 <https://doi.org/10.1029/2001JD000451>, 2002.

753 Whitby, K. T.: The physical characteristics of sulfur aerosols, *Atmos. Environ.*, 12, 135–159,  
754 <https://doi.org/10.1016/j.atmosenv.2007.10.057>, 1978.

755 Wiedensohler A.: An approximation of the bipolar charge distribution for particles in the submicron  
756 size range, *J. Aerosol Sci.*, 19, 387–389, [https://doi.org/10.1016/0021-8502\(88\)90278-9](https://doi.org/10.1016/0021-8502(88)90278-9), 1988.

757 Wu, G. X., Li, Z. Q., Fu, C. B., Zhang, X. Y., Zhang, R. Y., Zhang, R. H., Zhou, T. J., Li, J. P., Li, J.  
758 D., and Zhou, D. G.: Advances in studying interactions between aerosols and monsoon in China,  
759 *Science China Earth Science*, 59, 1–16, <https://doi.org/10.1007/s11430-015-5198-z>, 2016.

760 Wu, Z., Wang, Y., Tan, T., Zhu, Y., Li, M., & Shang, D., et al.: Aerosol liquid water driven by  
761 anthropogenic inorganic salts: implying its key role in the haze formation over north china  
762 plain, *Environ. Sci. Technol. Lett.*, 5(3), 160-166, <https://doi.org/10.1021/acs.estlett.8b00021>, 2018.

763 Xu, L., Guo, H., Boyd, C. M., Klein, M., Bougiatioti, A., Cerully, K. M., Hite, J. R., Isaacman-  
764 VanWertz, G., Kreisberg, N. M., Knote, C., Olson, K., Koss, A., Goldstein, A. H., Hering, S. V., de  
765 Gouw, J., Baumann, K., Lee, S.-H., Nenes, A., Weber, R. J., and Ng, N. L.: Effects of anthropogenic  
766 emissions on aerosol formation from isoprene and monoterpenes in the southeastern United States,  
767 *P. Natl. Acad. Sci.*, 112, 37–42, <https://doi.org/10.1073/pnas.1417609112>, 2015.

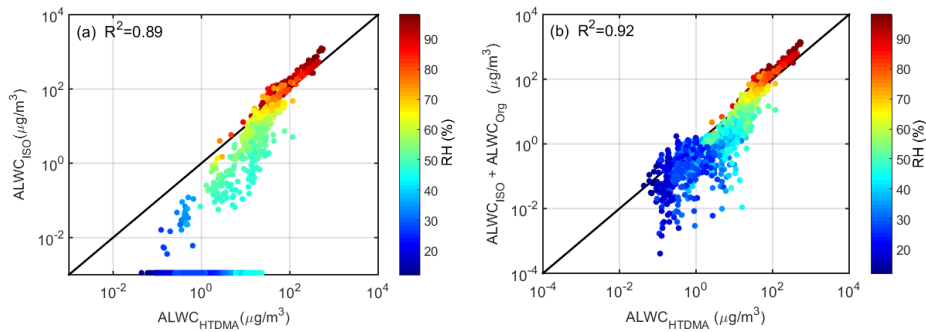
768 Xu, W., Han, T., Du, W., Wang, Q., Chen, C., Zhao, J., Zhang, Y., Li, J., Fu, P., Wang, Z., Worsnop, D.  
769 R., Sun, Y.: Effects of Aqueous- Phase and Photochemical Processing on Secondary Organic  
770 Aerosol Formation and Evolution in Beijing, China, *Environ. Sci. Technol. Lett.*, 51 (2), 762–770,  
771 <https://doi.org/10.1021/acs.est.6b04498>, 2017.

772 Zheng, B., Zhang, Q., Zhang, Y., He, K. B., Wang, K., Zheng, G. J., Duan, F. K., Ma, Y. L., Kimoto,  
773 T.: Heterogeneous chemistry: a mechanism missing in current models to explain secondary  
774 inorganic aerosol formation during the January 2013 haze episode in North China, *Atmos. Chem.*  
775 *Phys.*, 15 (4), 2031–2049, <https://doi.org/10.5194/acp-15-2031-2015>, 2015.

776 Zieger, P., Väisänen, O., Corbin, J. C., Partridge, D. G., Bastelberger, S., Mousavi-Fard, M., Rosati,  
777 B., Gysel, M., Krieger, U. K., Leck, C., Nenes, A., Riipinen, I., Virtanen, A., and Salter, M. E.:

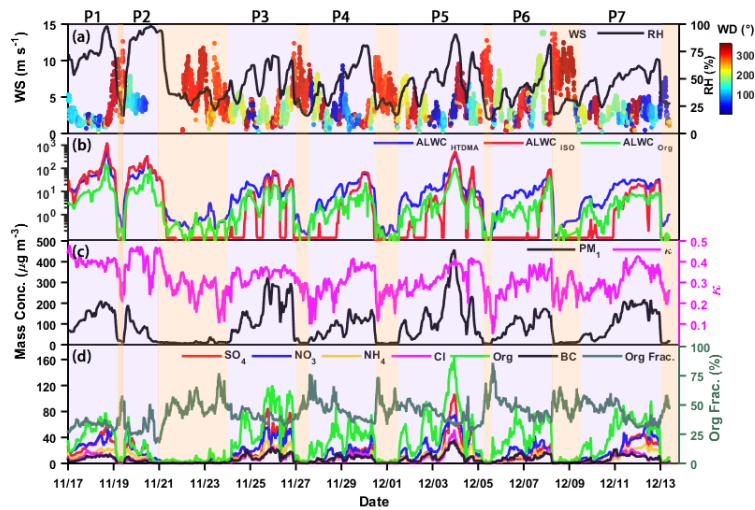
778 Revising the hygroscopicity of inorganic sea salt particles, Nature communications, 8, 15883,  
 779 <https://doi.org/10.1038/ncomms15883>, 2017.

780  
 781



782  
 783 **Figure 1.** Comparison between  $ALWC_{HTDMA}$  and (a)  $ALWC_{ISO}$  and (b) the sum of  $ALWC_{ISO}$  and  $ALWC_{Org}$ .  
 784  $ALWC_{HTDMA}$  refers to calculated ALWC based on the measured growth factor and PNSDs,  $ALWC_{ISO}$  refers to  
 785 simulated ALWC from the ISORROPIA II model, and  $ALWC_{Org}$  refers to the inferred ALWC contributed by  
 786 organic species. The coefficient of determination  $R^2$  is given in each panel. The color of the dots denotes the ambient  
 787 RH; the solid line denotes the 1:1 line.

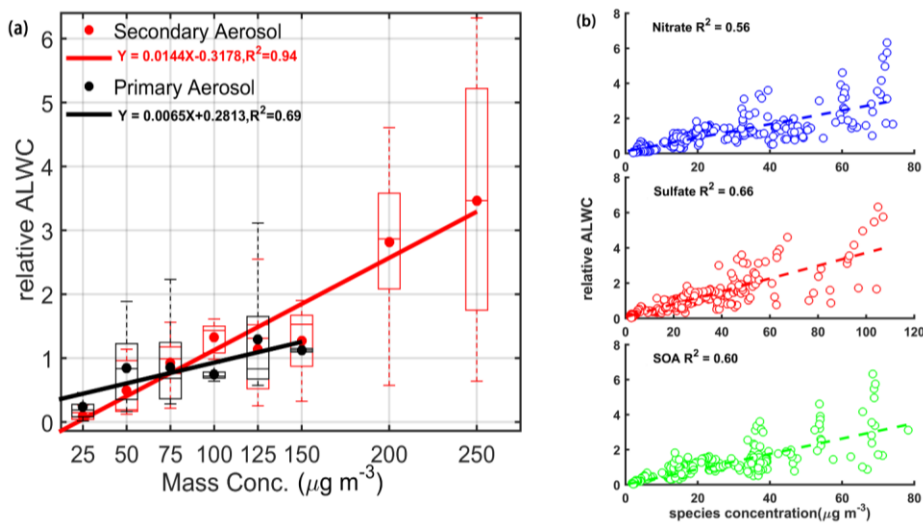
788



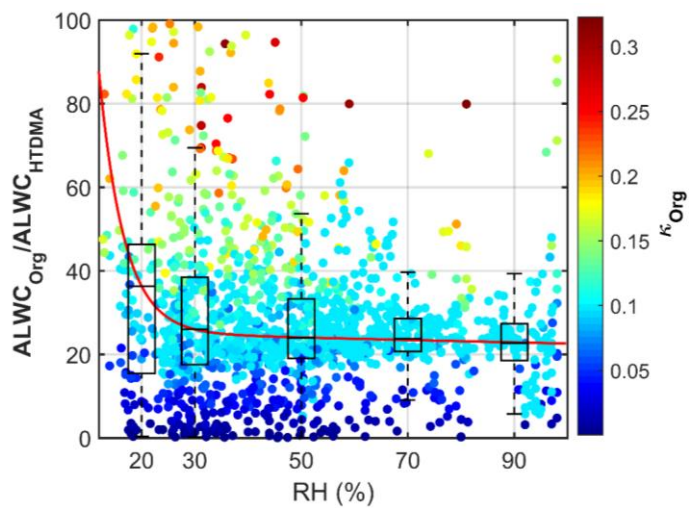
789  
 790 **Figure 2.** Time series of (a) wind speed (WS, left y-axis), ambient relative humidity (RH, right y-axis), and wind  
 direction (WD, right y-axis); (b)  $ALWC_{HTDMA}$ ,  $ALWC_{ISO}$ , and  $ALWC_{Org}$ ; (c)  $PM_{10}$  and  $K_c$ ; (d)  $SO_4$ ,  $NO_3$ ,  $NH_4$ , Cl, Org, BC, and Org Frac.

791 direction (WD, colored dots), (b)  $ALWC_{HTDMA}$  (in blue),  $ALWC_{ISO}$  (in red), and  $ALWC_{Org}$  (in green), (c)  $PM_{10}$  mass  
 792 concentration (left y-axis) and hygroscopicity parameter ( $\kappa$ , right y-axis) calculated using the ZSR model described  
 793 by Eq. (7), and (d) mass concentrations of aerosol species in  $PM_{10}$  (left y-axis) and organic aerosol mass fraction  
 794 (right y-axis). Seven polluted episodes (segments of the time series with a purple background) are selected for  
 795 examination.

796

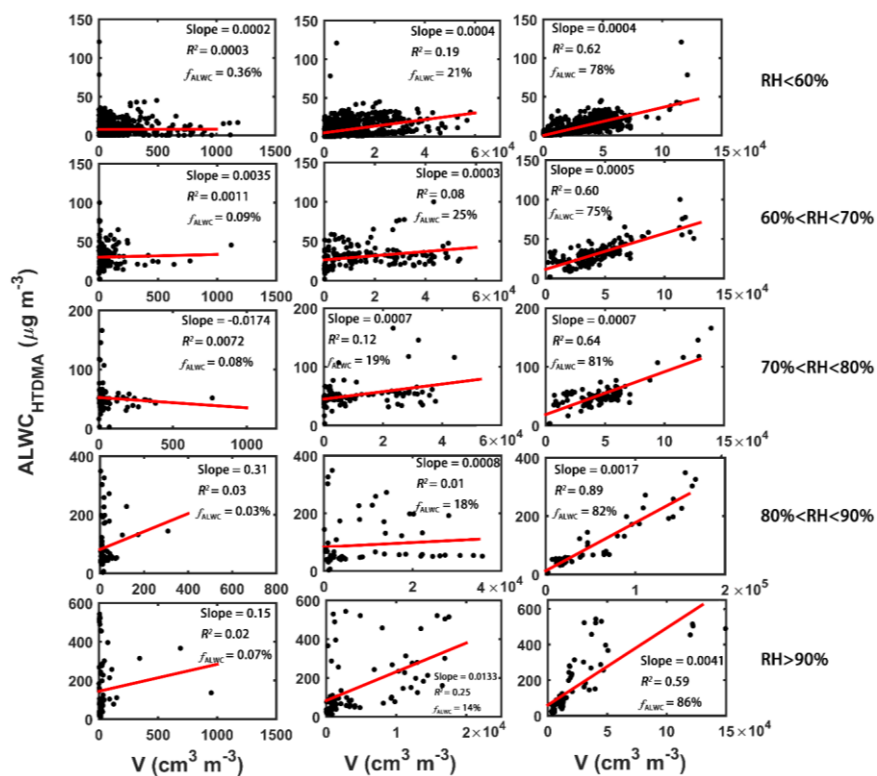


797  
 798 **Figure 3.** The correlation analysis between relative ALWC and (a) primary (in black) and secondary (in red) aerosol  
 799 mass concentrations, and (b) nitrate, sulfate, and secondary organic aerosol (SOA) mass concentrations. Panel (a)  
 800 shows mean relative ALWCs (solid dots) with boxes showing the 25th, 50th, and 75th percentiles. The extremities  
 801 show the 5th and 95th percentiles. The solid lines in (a) and the dashed lines in (b) both represent the corresponding  
 802 best-fit lines from linear regression.



803

804 **Figure 4.** The variation of the fraction of  $ALWC_{Org}$  in total  $ALWC$  ( $ALWC_{HTDMA}$ ) with the ambient relative humidity  
 805 **(RH).** The color of the dots denotes the hygroscopicity parameter of organics ( $\kappa_{Org}$ ). The boxes show the fraction of  
 806  $ALWC_{Org}$  with the 25th, 50th, and 75th percentiles. The extremities show the 5th and 95th percentiles. The red line  
 807 shows the fitting curve with the function  $y = ae^{bx}$ .

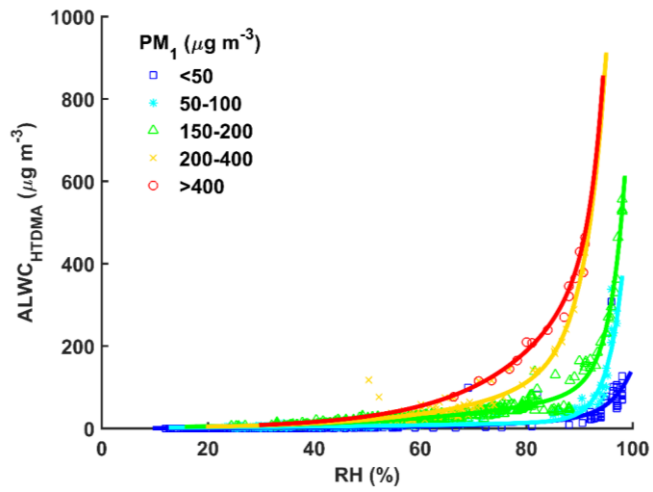


808

809 Figure 65. The correlation analysis between ALWC<sub>HTDMA</sub> and the volume concentration of nucleation mode (left  
 810 column), Aitken mode (middle column), and accumulation mode (right column) particles under different ambient  
 811 relative humidity (RH) conditions. The average contribution of each mode particles to ALWC under different  
 812 ambient RH conditions is denoted by f<sub>ALWC</sub>. The red lines represent the best-fit lines from linear regression.

813

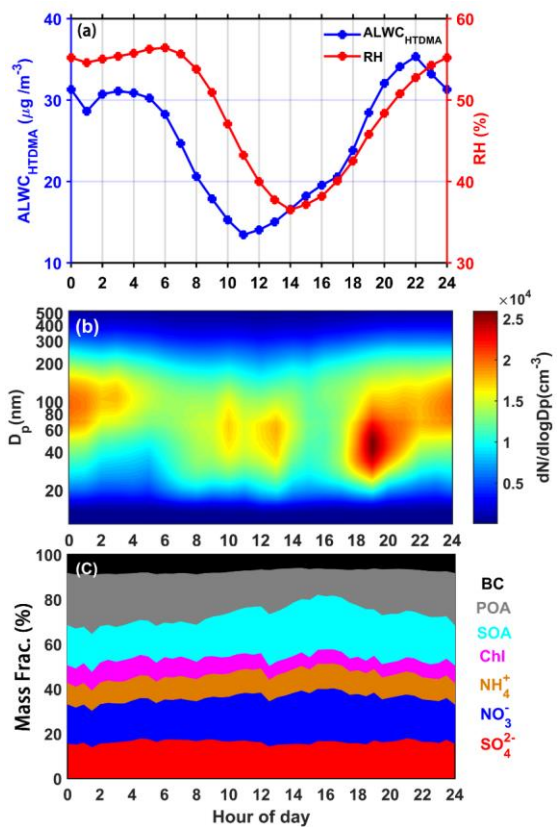




814

815 Figure 76. The dots show how  $ALWC_{HTDMA}$  varies with the ambient relative humidity (RH) for different  $PM_1$  mass  
 816 concentration ranges (colored symbols). The colored curves represent the best-fit lines through the data using the  
 817 fitting function  $y = ae^{bx}$ .

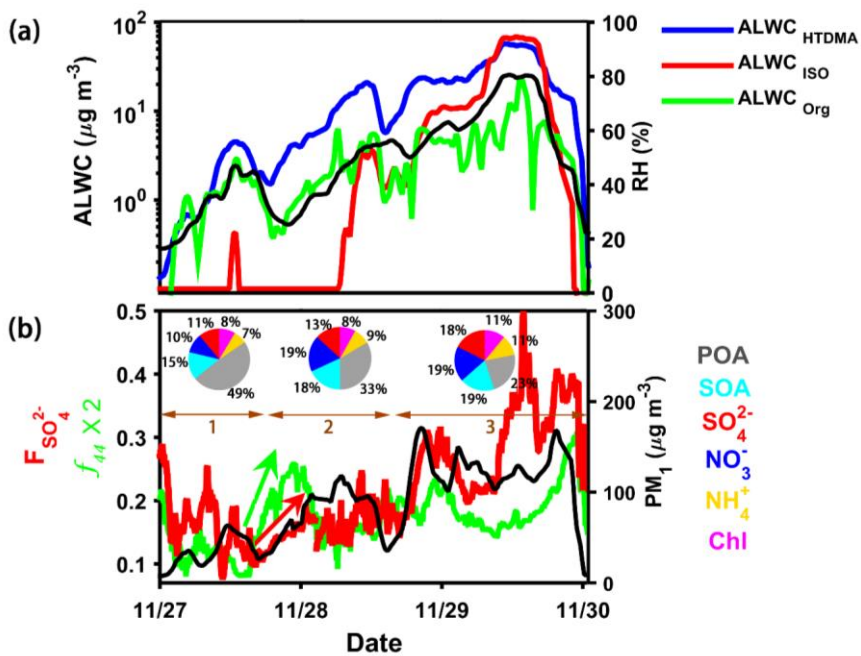
818



819

820 Figure 87. Diurnal variations of (a) ALWC<sub>HTDMA</sub> (in blue) and ambient RH (in red), (b) particle number size  
 821 distribution, and (c) the mass fraction of different chemical species. The time is in Beijing time.

822



823

824 Figure 98. Time series of (a)  $\text{ALWC}_{\text{HTDMA}}$  (in blue),  $\text{ALWC}_{\text{ISO}}$  (in red),  $\text{ALWC}_{\text{Org}}$  (in green), and RH (right y-axis),  
 825 and (b) the sulfur oxidation ratio ( $F_{\text{SO}_4^{2-}}$ ),  $f_{44}$ , and  $\text{PM}_{10}$  mass concentration (right y-axis) during the P4 case in Figure  
 826 2. The pie charts in (b) represent the average chemical compositions of  $\text{PM}_{10}$  during three stages of the pollution  
 827 event (denoted by brown horizontal lines). The red and green arrows in (b) indicate the rapid increase in  $F_{\text{SO}_4^{2-}}$  and  
 828  $f_{44}$  at the initial stage.

829